One-pot synthesis of water-dispersible Ag_2S quantum dots with bright fluorescent emission in the second near-infrared window

One-pot synthesis of water-dispersible Ag₂S quantum dots with bright fluorescent emission in the second near-infrared window

Hua-Yan Yang, Yu-Wei Zhao, Zheng-Yong Zhang, Huan-Ming Xiong and Shao-Ning Yu

Department of Chemistry, Fudan University, Shanghai 200433, People's Republic of China

E-mail: yushaoning@fudan.edu.cn and hmxiong@fudan.edu.cn

Abstract

The second near-infrared window (NIR-II, wavelength of 1.0–1.4 μm) is optimal for the bioimaging of live animals due to their low albedo and endogenous autofluorescence. Herein, we report a facile and one-pot biomimetic synthesis approach to prepare water-dispersible NIR-II-emitting ultrasmall Ag₂S quantum dots (QDs). Photoluminescence spectra showed that the emission peaks could be tuned from 1294 to 1050 nm as the size of the Ag₂S QDs varied from 6.8 to 1.6 nm. The x-ray diffraction patterns and x-ray photoelectron spectra confirmed that the products were monoclinic α-Ag₂S. Fourier transform infrared spectrograph analysis indicated that the products were protein-conjugated Ag₂S QDs. Examination of cytotoxicity and the hemolysis test showed that the obtained Ag₂S QDs had good biocompatibility, indicating that such a nanomaterial could be a new kind of fluorescent label for *in vivo* imaging.

S Online supplementary data available from stacks.iop.org/Nano/24/055706/mmedia

(Some figures may appear in colour only in the online journal)

1. Introduction

In 2003, simulations and modeling studies on optical imaging in tissues or blood suggested that improving the signal-to-noise ratio by more than 100 fold was possible by using quantum dots that emitted light at 1320 nm (instead of 850 nm) [1]. Further research disclosed that the second near-infrared window (NIR-II) was optimal for the optical imaging of live animals due to their much lower albedo and endogenous autofluorescence in this wavelength range than in the NIR-I window (700–950 nm) [2–4]. However, the lack of biocompatible fluorescent probes in the NIR-II region prevented the utilization of this highly sensitive spectral range for *in vivo* imaging. There have been very few reports concerning such fluorescent probes in the past decade. For example, single-walled carbon nanotubes (SWNTs) were reported as promising candidates for biological imaging and sensing due to their unique fluorescence in the NIR-II window, but their photoluminescent quantum yield (QY) was rather low, which limited their practical applications [5–7]. Therefore, the development of stable and highly luminescent probes in the NIR-II window is required urgently.

Quantum dots (QDs) have received great attention as biological labeling agents due to their distinguished luminescent properties, including high QY, size-dependent emission and symmetric emission spectra [6, 8–11]. However, conventional NIR-II QDs, such as PbS [12], PbSe [13], PbTe [14], InP [15] and CdHgTe [16], contain highly toxic compounds that limit their applications *in vivo*. In addition, these NIR-emitting QDs are usually prepared in organic phase, and additional surface modification is employed to render them water-dispersible for biological

applications [11, 17–22]. Therefore, synthesizing nontoxic NIR-emitting QDs directly in aqueous solution will greatly simplify the preparation.

Silver sulfide is known to exist in several different allotropic forms, including α-Ag$_2$S (achantite, monoclinic, stable up to 178°C), β-Ag$_2$S (argentite, bcc, stable between 178°C and 600°C) and γ-Ag$_2$S (fcc, stable above 600°C), and it has potential applications in photoconducting cells, photovoltaic devices and IR detectors [23]. Nanoscaled α-Ag$_2$S is a promising candidate for NIR probes due to its bulk bandgap of 0.85 eV [24, 25] and negligible toxicity [26]. Although several reports on using Ag$_2$S QDs as biomarkers have been published recently, only a few of them concerned Ag$_2$S NIR-II emission [25, 27–31]. Zhang *et al* [3, 32] reported a kind of α-Ag$_2$S synthesized in organic phase at 160–180°C that exhibited only one emission maximum at 1050 nm, but the products should be transferred to the aqueous solution for bioimaging. To our knowledge, there is no literature reporting one-pot synthesis of water-dispersible Ag$_2$S QDs with NIR-II-emitting properties so far.

Recently, various biological molecules including amino acids, peptides, proteins, DNA, and RNA, have been used for the synthesis of various nanomaterials due to their ability to influence the nucleation and growth of nanoparticles [33–35]. The biomolecule-conjugated nanomaterials were more suitable for bioapplications owing to their bioactive surface [36]. Bovine serum albumin (BSA) is the most studied protein, and it has a strong affinity to a variety of inorganic molecules binding to different sites, which makes possible the utilization of BSA-decorated nanomaterials in a variety of supramolecular assemblies [33]. In this work, BSA was used as a capping agent to grow Ag$_2$S QDs. AgNO$_3$ was incubated with BSA for the initial heterogeneous nucleation, followed by a slow injection of Na$_2$S solution through a syringe pump. After agitation for Ag$_2$S crystallization, the product was purified by dialysis. The whole procedure was conducted at room temperature and in aqueous solutions, and was efficient in energy and friendly to the environment. These Ag$_2$S QDs had ultrasmall sizes (<10 nm) and exhibited size-dependent emission wavelengths from 1050 to 1294 nm. Cytotoxicity and hemolysis measurements confirmed the excellent biocompatibility of such Ag$_2$S QDs.

2. Materials and methods

2.1. Materials

AgNO$_3$, Na$_2$S·10H$_2$O and BSA (purity 98%, $M_w = 68\,000$) were all from the Chinese Sinopharm Chemical Reagent Co., Ltd. Styryl-13 (LDS925) was purchased from Exciton, USA. Thiazolyl blue tetrazolium bromide (MTT) was purchased from Sigma-Aldrich (Milwaukee, USA). RPMI-1640 medium, fetal bovine serum, penicillin, streptomycin, trypsin and EDTA were purchased from the domestic market. Methanol (Merck, A.R.) was used as received and double distilled water was used throughout.

2.2. Synthesis of the Ag$_2$S QDs

In a typical reaction, 25 ml of 4 mM AgNO$_3$ aqueous solution was added to 50 ml of 2 mg ml^{-1} BSA aqueous solution with vigorous stirring at room temperature to obtain the BSA–Ag$^+$ complex. This chelating reaction continued in the dark overnight under stirring. Next, 25 ml of 8 mM Na$_2$S aqueous solution was injected into the flask using a syringe pump with a delivery rate of 480 μl min^{-1}. After a few minutes, the mixture turned brownish yellow in color. The final solution was clear dark brown and purified through a 10 kDa dialysis membrane for 2 days with 6 changes of distilled water per day. Then the dialyzed solutions were centrifuged to precipitate the protein–QDs complex. The precipitate was washed with distilled water, transferred to a new vial, and centrifuged and washed again. This procedure was repeated three times. After the third washing step the supernatant did not contain any detectable amounts of protein. The final solution was collected and freeze dried to form a black solid product that was redispersed in distilled water or phosphate buffered saline buffer (PBS) for further use. Several replicas of the control experiment were conducted in parallel. The Ag$_2$S QDs with different sizes were obtained by keeping the concentration of Ag precursor and changing the concentration of the S precursor.

2.3. Characterization of the Ag$_2$S QDs

Transmission electron microscopy (TEM) and energy-dispersive x-ray (EDX) spectroscopy analysis were all performed on a JEM-2010 transmission electron microscope. Samples were prepared by dipping a carbon-coated copper grid into water containing the Ag$_2$S QDs, and the solvent evaporated at room temperature into the air. HRTEM was carried out on a field emission transmission electron microscope (JEOL JME-2100F). X-ray powder diffraction (XRD) measurements were obtained by a Bruker D8 Advance x-ray powder diffractometer using Cu Kα radiation wavelength of 0.154 056 nm and a scan rate of 8° min^{-1}. X-ray photoelectron spectroscopy (XPS) was carried out on a Perkin Elmer RBD upgraded PHI-5000CESCA system using Mg Kα radiation or Al Kα radiation. The concentrations of the obtained Ag$_2$S solutions were determined by a Thermo E. IRIS Duo inductively coupled plasma–atomic emission spectroscopy (ICP-AES) detector. UV–vis–NIR adsorption spectra measurements were carried out on an HP 8453 UV–vis–NIR absorption spectrometer. The near-infrared photoluminescence of the Ag$_2$S solution was measured using a near-infrared spectrometric analyser with the excitation light provided by a fiber-coupled 648 nm diode laser and the fluorescence signal collected by a BTC261E-512-element InGaAs spectrometer (B&WTEK company, China). The infrared spectra were obtained from a Nicolet Avatar 470 Fourier transform infrared spectrometer in the wavenumber range of 4000–400 cm^{-1}. Dynamic light scattering (DLS) and zeta-potential data were acquired from a MALVERN Zetasizer, Nano-ZS (Malvern Instruments, UK).

The QY of the Ag$_2$S QDs was calculated using styryl-13 ((2-[*p*-dimethylaminophenyl)-2,4-neopentylene-1,3,5,7-octatetraenyl]-3-ethyl-(6,7-benzo)-benzothiazolium perchlorate) as a reference dye (QY = 11%) according to Crochet *et al* [7]. The sample's QY was determined based on equation (1),

$$\eta_s = \eta_{ref} \times (I_s/I_{ref}) \times (A_{ref}/A_s) \times (n_s/n_{ref})^2 \qquad (1)$$

where η_{ref} is the QY of the reference (styryl-13), I is the integrated emission intensity, A is the absorption value at the excitation wavelength and n is the refractive index of the solvent. Refractive indices n_s for water and n_{ref} for methanol are similar and do not need to be taken into account.

2.4. Cell cultivation and cytotoxicity assay

Human intestinal epithelial cells (HIEC) were cultured with RPMI-1640 medium supplemented with 10% fetal bovine serum and 1% penicillin streptomycin solution (10 000 units of penicillin and 10 mg of streptomycin in 1 × PBS) in a humidified atmosphere of 5% CO$_2$, 95% air at 37°C. Cells were cultured in 96-well plates (100 μl of cell solution per well). The optimum cell concentration as determined by the growth profile of the cell line was 1×10^4 cells ml^{-1}. Cells were incubated for 24 h before treatment with Ag$_2$S QD solution. The stock solution of Ag$_2$S QDs was prepared with 1 × PBS at a concentration of 2250 mg ml^{-1} (Ag$_2$S by weight, w/w), which was determined by ICP-AES using the external standard method. HIEC were treated with 0–300 μg ml^{-1} of the QD solution for 24 h and the Ag$_2$S QD solution was diluted with the above medium.

2.5. MTT assay

Cytotoxicity was evaluated by performing 3-(4,5-dimethyl-thiazol-2yl)-2,5-diphenyltetrazolium bromide (MTT) assays on the HIEC. The 96-well culture plates were seeded with 10^4 cells in culture medium at 37°C and 5% CO$_2$ for 24 h. Next, the cells were incubated with different concentrations (0, 10, 50, 100, 200 and 300 μg ml^{-1}) of the Ag$_2$S QDs for another 24 h. After that time, the Ag$_2$S solution was discarded and the cells were washed twice with PBS. Then fresh culture medium (100 μl) and MTT (20 μl, 5 mg ml^{-1}, dissolved in 1 × PBS) were added to each well and the plate was incubated for another 4 h at 37°C. DMSO (150 μl) was added to each well to dissolve the purple formazan, with gentle shaking for 15 min so that complete dissolution was achieved. The absorbance of MTT at 490 nm was measured with an automatic ELISA analyzer (SPR-960).

2.6. Hemolysis test

The hemolysis test was performed according to ISO 10993-4:2002. Rabbit blood (8 ml) was immediately mixed with 10 ml of normal physiological saline containing sodium citrate (3.8 wt%) in a ratio of 9:1 and centrifuged at 2500 rpm for 10 min. The supernatant was discarded. The erythrocytes

were washed until the supernatant was clear, and the packed cells were dispersed in normal physiological saline to form a 2 wt% erythrocyte suspension. The Ag$_2$S QDs were re-dissolved in normal physiological saline to obtain 20, 40, 80 and 100 μg ml^{-1} sample solutions for hemolytic assay. A 5 ml aliquot of Ag$_2$S QDs dissolved in normal physiological saline at different concentrations, 5 ml of deionized water and 5 ml of normal physiological saline were used as a test group, positive control group and negative control group, respectively. Six parallel samples were prepared in each group. All tubes were put into the 37°C thermostatic water bath for 1 h. Next, the tubes were centrifuged for 10 min (2500 rpm) and the supernatants were used to measure the absorbance at 545 nm. Finally, the hemolytic ratio was expressed as a percentage and calculated using the mean value A for each group by equation (2):

$$\text{Hemolytic ratio (\%)} = \frac{(A_{test} - A_{negative\ control})}{(A_{positive} - A_{negative\ control})} \times 100. \qquad (2)$$

The test sample was considered hemolytic if the ratio was over 5%.

3. Results and discussion

One of the fundamental processes involved in biological mineral deposition is that the organic matrix (proteins or other biological macromolecules) controls the nucleation and growth of the inorganic structures [37–41]. Several studies have demonstrated that proteins can be used as templates for material synthesis *in vitro* [38, 41–44]. Biomolecules are effective ligands for inorganic nanomaterials through functional groups, such as amine, thiol and phosphate, chelating metal ions during synthesis and passivating nanoparticle surfaces after synthesis [45, 46]. In the present work, BSA is incubated with AgNO$_3$ under ambient conditions to form coordination between Ag$^+$ and BSA and facilitate heterogeneous nucleation. Moreover, a BSA coating on the Ag$_2$S QDs makes the product water-dispersible and biocompatible. In general, obtaining Ag$_2$S QDs directly in water is very difficult because the extremely low solubility of the Ag$_2$S ($K_{SP} = 6.3 \times 10^{-50}$) results in fast crystal growth. However, using biomimetic synthesis, the particle size of the Ag$_2$S QDs can be controlled by changing the precursor molar ratio of Ag to S.

3.1. Changing experimental parameters to prepare emission-tunable Ag$_2$S QDs

The optical properties of QDs are size-dependent; thus, size control is crucial for tuning the photoluminescence wavelength. The TEM images show that the obtained QDs are quasi-spherical particles with a narrow size distribution (figure 1). By tuning the precursor molar ratio of Ag to S (3:1, 1:2, 1:3, 1:5, 1:10), uniform Ag$_2$S QDs were obtained with average diameters of 1.6, 3.3, 3.7, 5.0 and 6.8 nm, respectively. UV–vis absorption and PL spectra of the as-prepared Ag$_2$S QDs are compared in figure 2. Pure
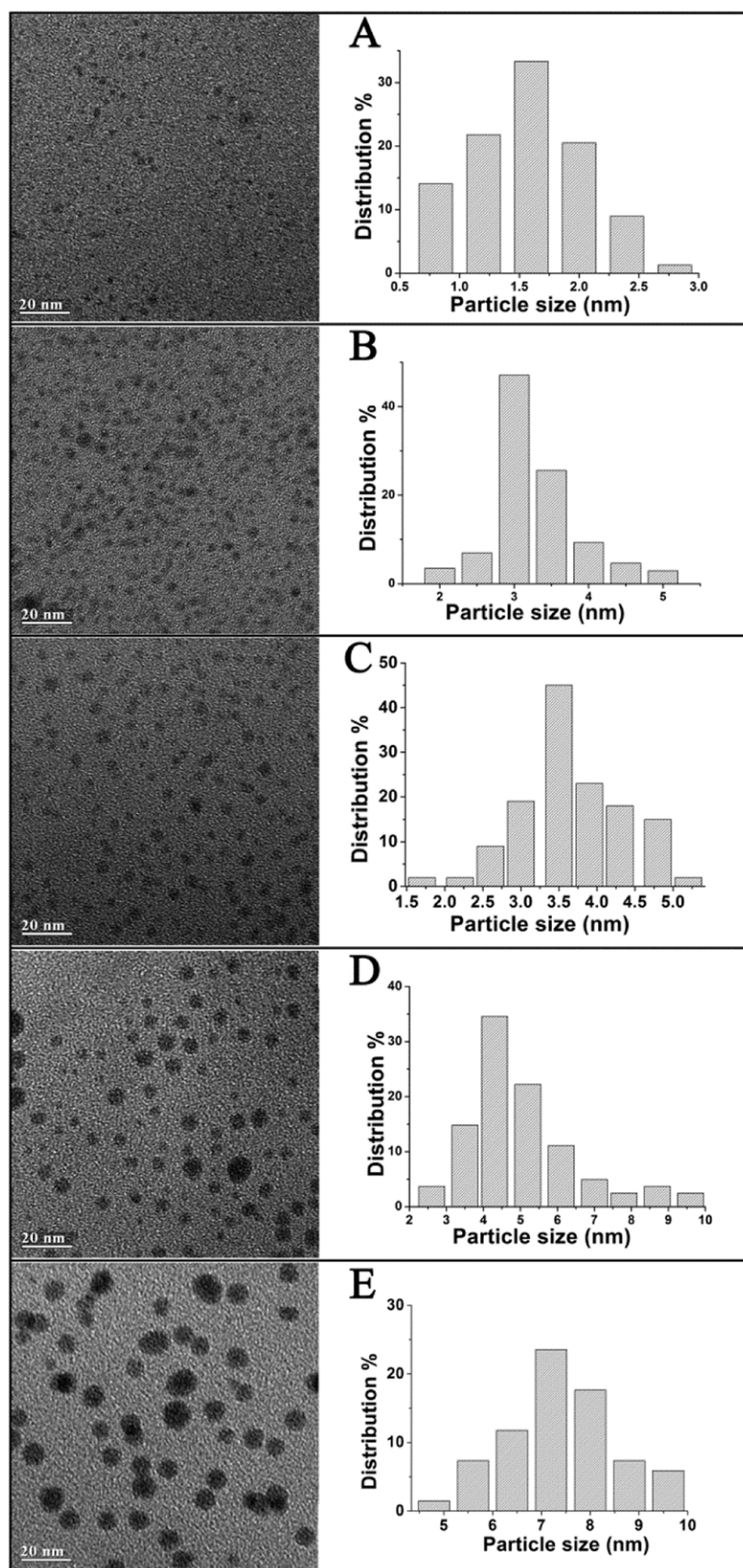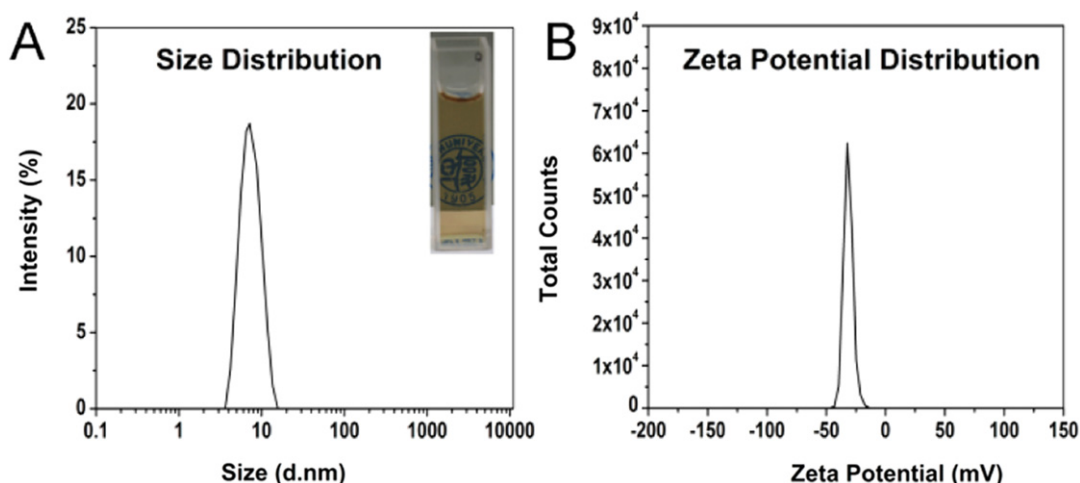
Figure 1. TEM images (left) and size distribution graphs (right) of the Ag_2S QDs synthesized by different Ag/S molar ratios. (A) 3:1, (B) 1:2, (C) 1:3, (D) 1:5 and (E) 1:10.
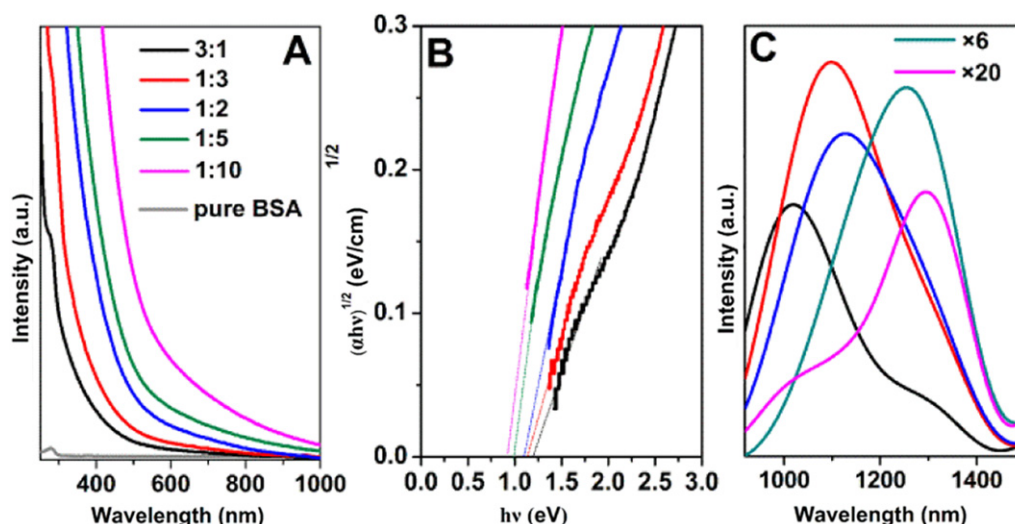
Figure 2. (A) UV–vis–NIR absorbance spectra of the QDs in water synthesized by different Ag/S molar ratios: (a) 3:1, (b) 1:2, (c) 1:3, (d) 1:5, (e) 1:10, and (f) pure BSA in water. (B) $(\alpha h\nu)^{1/2}$ as a function of photon energy ($h\nu$) for Ag$_2$S QDs and (C) their NIR PL spectra.

Figure 3. (A) Dynamic light scattering spectra and photograph and (B) zeta-potential measurements of BSA capped Ag$_2$S QDs in aqueous solution.

BSA shows a weak absorption band of protein at about 280 nm (figure 2(A)), while the absorption spectra of the Ag$_2$S QDs are much stronger in the UV–vis region and extend to the near-infrared region. This result is close to that of the Ag$_2$S nanoparticles with similar sizes synthesized from organic solvents [25, 47]. The bandgap energies of the QDs with different sizes can be deduced via the Bardeen or Tauc equation (3) [25, 48]:

$$(\alpha h\nu)^{1/n} = A(h\nu - E_g) \qquad (3)$$

where α is the absorption coefficient, h is Planck's constant, ν is the frequency of vibration, α is the absorption coefficient, E_g is the bandgap, and A is a proportional constant. The value of the exponent n denotes the nature of the electron transition of the sample. For the indirect allowed transition, $n = 2$. Extrapolation of the line to the baseline, where the value of $(\alpha h\nu)^{1/2}$ is zero, will give the E_g value (figure 2(B)). The estimated E_g values of these Ag$_2$S QDs with average diameters of 1.6, 3.3, 3.7, 5.0 and 6.8 nm are

approximately 1.23, 1.16, 1.12, 1.02 and 0.94 eV, respectively. This result confirms that the bandgaps of Ag$_2$S QDs are size-dependent, and these E_g values are larger than that of the bulk material (0.85 eV) [25, 49]. Figure 2(C) depicts the NIR photoluminescence spectra of Ag$_2$S QDs excited by a 648 nm laser diode. As the Ag/S molar ratio decreases, the PL emission maximum of the Ag$_2$S QDs shifts from 1294 to 1050 nm. Compared with the bulk Ag$_2$S [24, 47], the PL emission of our Ag$_2$S QDs shows a shift to the higher energy due to the quantum size effects. We chose the product derived from the Ag/S molar ratio of 1:2, which exhibited the highest QY of 1.8%, as the typical sample for further characterization and biological experiments.

3.2. Characterization of Ag$_2$S QDs

The dynamic light scattering (DLS) measurement showed that the hydrodynamic diameter of the QDs in water is approximately 10 nm (figure 3(A)). The difference in diameter

Table 1. The main IR absorption bands for the pure BSA and the BSA–Ag$_2$S QDs.

Designation	Pure BSA (cm^{-1})	BSA–Ag$_2$S (cm^{-1})	Description
Amide A	3295	3490	NH stretching
C–H stretching	2960	2956	Alkyl C–H stretching
Amide I	1658	1662	C=O stretching
Amide II	1535	1544	CN stretching, NH bending
CH$_2$, CH$_3$ bending	1392	1394	CH$_2$, CH$_3$ bending
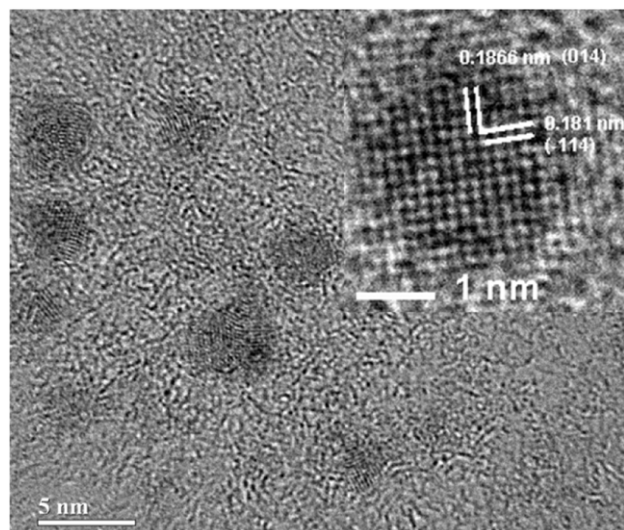
Figure 4. HRTEM images of Ag$_2$S synthesized in a typical experiment.

measured by TEM (average particle size is about 3.3 nm) and DLS could be attributed to the different surface species of the as-prepared QDs in aqueous phase. Such small size of the fluorescent probes offers great advantages for bioapplications. Zeta-potential measurements of the Ag$_2$S QD solution (0.1 mM in water) gave a slightly negative surface charge (−31.1 eV, figure 3(B)), indicating that the surface charge was dominated by the bound BSA. The Ag$_2$S QDs dispersed in water (figure 3(A), inset), which showed no obvious flocculate in the water at room temperature upon standing for several months. It is likely that the surface-bound BSA prevented aggregation and growth of the QDs.

To evaluate the crystalline states and composition of the selected sample, HRTEM, XRD and XPS measurements were carried out. HRTEM (figure 4) showed that the nanoparticles had clear crystal structures and obvious lattice planes. The lattice planes of the focused nanocrystal with a *d*-space of 0.1866 nm and 0.181 nm in nanocrystals could be indexed as the (014) plane and ($\bar{1}$14) plane of monoclinic Ag$_2$S nanocrystals. The XRD patterns of the as-prepared Ag$_2$S QDs were weak and undistinguishable, because the QDs were too small and coated by plenty of amorphous ligands. Hence, we treated the sample at 70°C under N$_2$ gas flow for 12 h and scanned the XRD patterns of this sample. Figure 5(A) shows that the Ag$_2$S crystallinity is significantly improved and the XRD peaks match well with the monoclinic α-Ag$_2$S data (JCPDS Card No. 14-0072). The XPS spectrum (figure 5(B)) proves the presence of Ag and S, as well as C, O and N

elements. C 1s (284.0 eV) is chosen as the reference line. The peaks at 367.8 and 373.6 eV in figure 5(C) can be assigned to the core levels of Ag 3d$_{5/2}$ and Ag 3d$_{3/2}$, which indicates that the oxidation state of the Ag ion is univalent in the Ag$_2$S QDs [50]. The spectrum of S 2p shown in figure 5(D) could be described as three peaks located at about 161.2, 162.4 and 164.4 eV, respectively. The peaks at 162.4 and 161.2 eV can be assigned to the binding energies of S 2p$_{1/2}$ and S 2p$_{3/2}$, respectively, which are separated by a spin–orbit splitting of 1.2 eV [51, 52]. The peak at 164.4 eV can be also assigned to the sulfur [53], which might be from the thiol groups of the protein molecules on the Ag$_2$S surface. The actual Ag/S atomic ratio on the QD surface is roughly 1.75:1, indicating that sulfur is slightly excessive. Energy-dispersive x-ray (EDX) data (figure 5(E)) confirmed that the products consisted of the elements Ag and S with an atomic ratio of 1.89:1, which was consistent with the XPS results and close to the stoichiometry of bulk Ag$_2$S.

FT–IR spectra of the pure BSA and the BSA–Ag$_2$S products are compared in figure 6 and table 1. According to our previous reports [54], the IR peaks of the pure protein at 3295, 1658 and 1535 cm^{-1} are assigned to the stretching vibrations of the amide A (mainly –NH stretching vibration), amide I (C=O stretching) and amide II (CN stretching, NH bending). The peaks at 2960 and 1392 cm^{-1} are assigned to CH$_2$ and CH$_3$ stretching and bending. Comparing the IR spectrum of BSA–Ag$_2$S with that of the pure BSA, there are negligible variations in the characteristic peaks of –CH$_3$ groups and amide I bands, but the characteristic peak of the amide II band shifts to a higher wavenumber by 11 cm^{-1}, suggesting that there might be a coordination interaction between the silver ions and BSA. Most notably, the characteristic peak of the amide A band shifts to a higher wavenumber of 3490 cm^{-1}. Such large variation further suggests that coordination has formed between QDs and the amine groups of BSA, which plays an important role in the formation of Ag$_2$S nanoparticles. Therefore, the FT–IR measurement proves that BSA ligands are conjugated to the Ag$_2$S QDs and probably responsible for the BSA–Ag$_2$S QD formation.

3.3. Study of formation mechanism of the Ag$_2$S QDs

To investigate the influence of BSA on the formation of the Ag$_2$S QDs, two sets of control experiments were carried out. Control A was synthesized in the absence of BSA (see figure S1 available at stacks.iop.org/Nano/24/055706/mmedia), in which shapeless and aggregated Ag$_2$S particles were generated. The result showed that BSA was a key factor
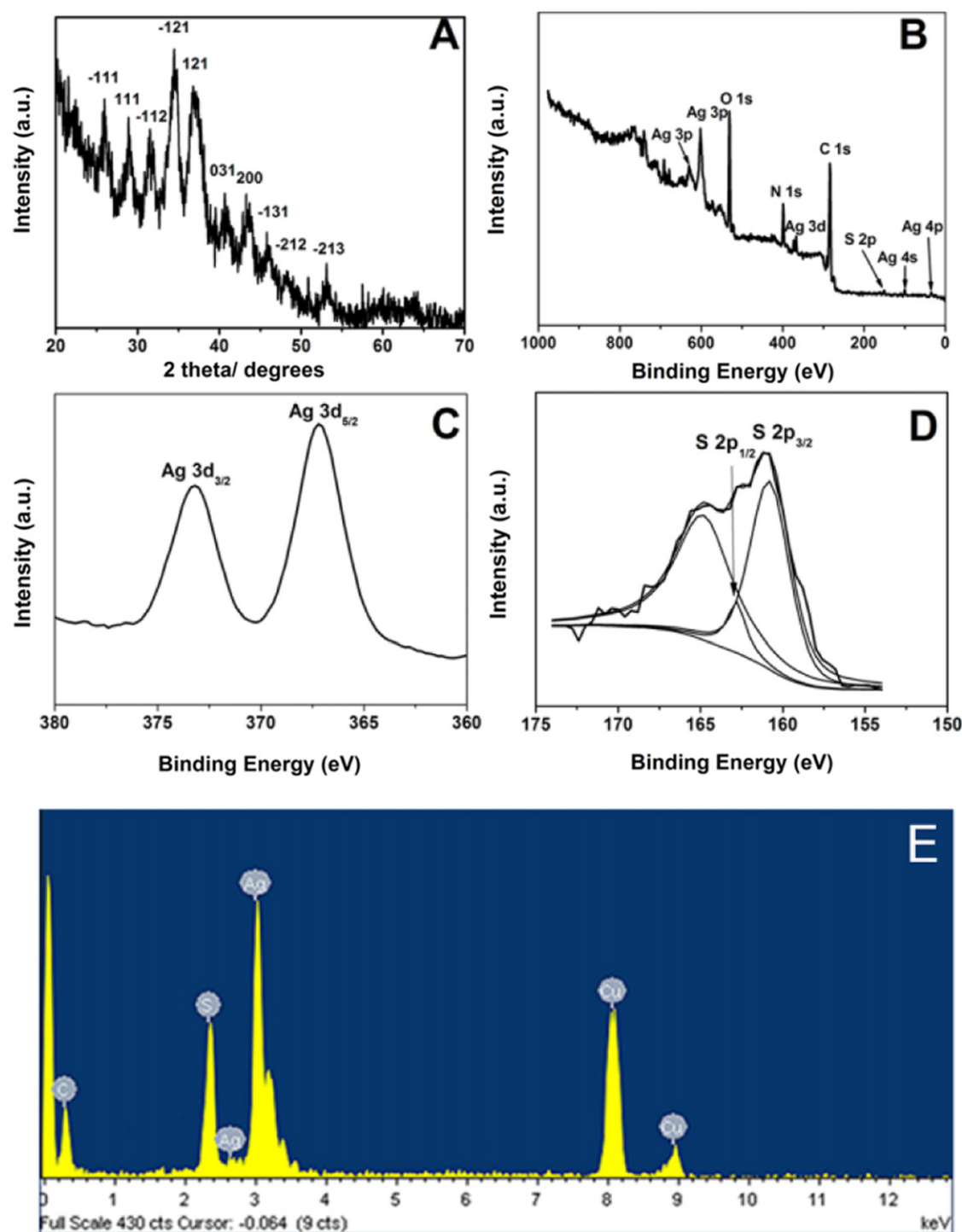
Figure 5. (A) XRD patterns of the Ag_2S QDs aged at 70°C for 12 h. The XPS spectra of (B) the whole survey, (C) Ag3d and (D) S 2p of the as-prepared Ag_2S QDs, (E) EDX spectrum collected for Ag_2S QDs.

in controlling and regulating the formation of the Ag_2S QDs. Control B was synthesized in the same conditions as those for the typical experiment, except that the chelating time between BSA and Ag^+ was zero. The TEM image shows that the obtained Ag_2S nanoparticles aggregated badly (figure S2 available at stacks.iop.org/Nano/24/055706/mmedia).

It is worth noting that the photoluminescence spectra of the two control samples and typical sample also show differences in the relative emission intensity (figure S4 available at stacks.iop.org/Nano/24/055706/mmedia). The products in control A shows no PL emission peak. The PL emission peak of the products in control B were weaker than in the typical experiment, which indicated that the appropriate chelating time between BSA and Ag^+ is of great importance to achieve desirable products.
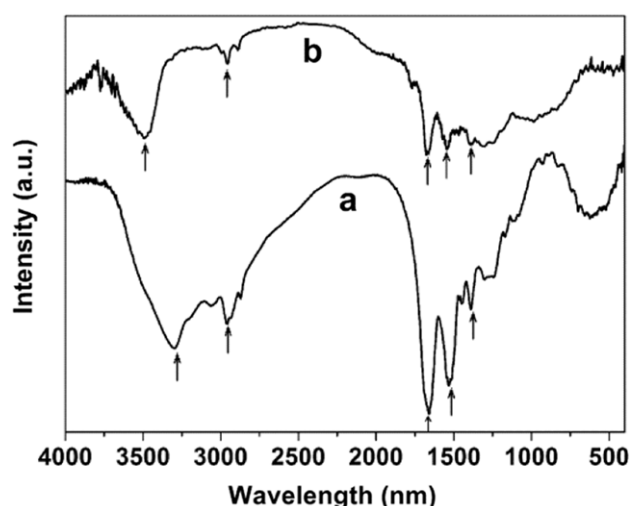
Figure 6. FT–IR spectra of (a) the obtained BSA–Ag$_2$SQDs and (b) the pure BSA dispersed in water.
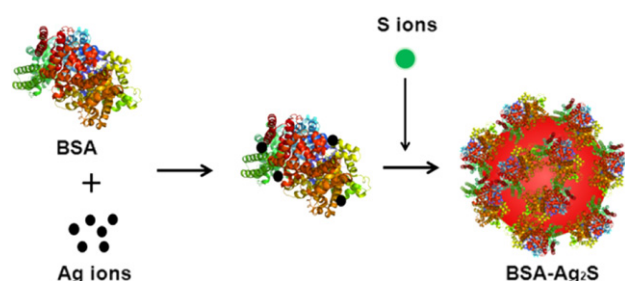

Scheme 1. Proposed formation mechanism of the Ag$_2$S QDs.

In summary, according to the above results, the key step of this synthetic protocol is that BSA bound to free Ag$^+$ strongly through the functional groups to form a Ag$^+$–BSA complex, which generates supramolecular aggregates that mimic the biological crystal growth environment. Therefore, BSA is able to promote nucleation and then stabilize the final products. The formation of protein-conjugated Ag$_2$S QDs is illustrated in scheme 1. First, protein bound to free Ag$^+$ strongly to form a Ag$^+$–BSA complex. Then, after adding sulfur ions, the Ag$_2$S nanocrystals formed. In the meantime, the conjugated protein stabilized the nanostructures and helped Ag$_2$S nanocrystals disperse in the water.

3.4. Toxicity and biocompatibility of the Ag$_2$S QDs

The cytotoxicity and biocompatibility of the nanomaterials should be considered first before any biological applications. In our studies, the cytotoxicity of the Ag$_2$S QDs in normal cells was evaluated using standard cell viability protocols. HIEC is a kind of normal cell without over-expressed or under-expressed receptors, so they are more objective for assessing the cytotoxicity of Ag$_2$S QDs in comparison with cancer cell lines that possess over-expressed membrane receptors. Figure 7 shows the viability of the cells labeled with six different concentrations of the Ag$_2$S QDs. Cell viability was more than 80% after 24 h of incubation with 300 μg ml^{-1}
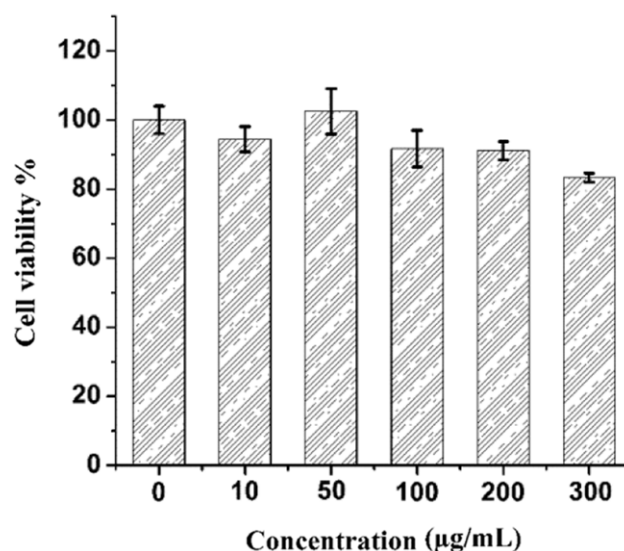

Figure 7. Cell viability of the Ag$_2$S QDs at different concentrations. The data are presented as mean $\pm$ SD ($n = 6$).

of the Ag$_2$S QD solution. This result indicates that our Ag$_2$S QDs are very safe for living cells. Furthermore, Ag$_2$S QDs were also incubated with tumor cells. After washing with PBS to remove unbound QDs, the labeled cells also show an obvious emission peak, which is consistent with Ag$_2$S QDs. No signal was detected from the control tumor cell alone. These observations demonstrated that the Ag$_2$S QDs can be swallowed by tumor cells and can be used for cell imaging. The detailed experimental process and figure (figure S5 available at stacks.iop.org/Nano/24/055706/mmedia) are deposited in supporting information.

Determination of hemolytic properties is one of the most common tests in studies of nanoparticle interactions with blood components [55]. Erythrocyte interaction with nanocrystals is particularly important in the application of nanocrystals for biological applications [56]. The hemolysis values of our tested samples are shown in table 2. According to ISO 10993-4:2002, the upper limit value of the hemolysis index is 5%. Thus, the BSA–Ag$_2$S QDs at the tested concentration exhibited no hemolysis. As shown in figure 8, the supernatant from BSA–Ag$_2$S QDs at different concentrations is achromatic, implying that no hemolysis occurred.

4. Conclusions

Many functional materials are produced naturally in the normal environment. Mimicking nature's methods of biological manufacture, we synthesized NIR-II-emitting ultrasmall Ag$_2$S QDs directly in aqueous phase through a facile one-pot sol–gel route at room temperature. This synthetic method was very simple and mild, and it was suitable to produce functional materials with proteins. The emission band of the as-prepared BSA–Ag$_2$S QDs could be tuned across the NIR-II region. Cytotoxicity and hemolysis tests proved that these Ag$_2$S QDs had good biocompatibility,
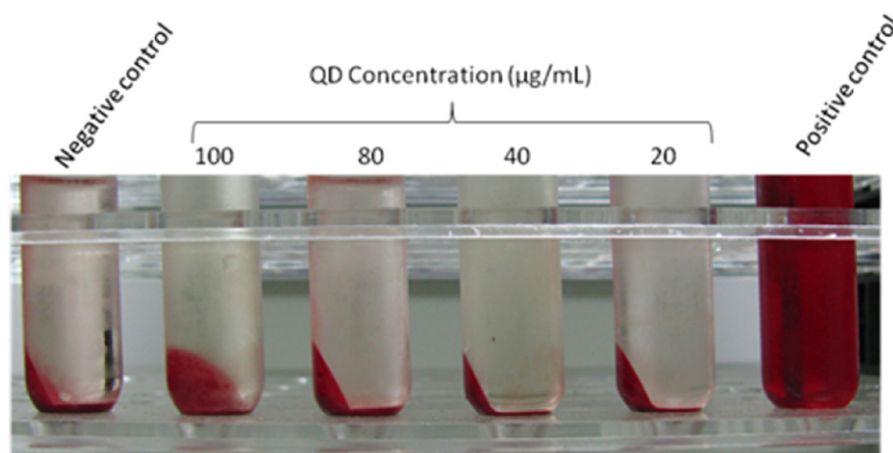
Figure 8. Photograph of the hemolysis test of the BSA–Ag$_2$S QDs with different concentrations, the positive control (2 wt% erythrocyte suspension in deionized water) and negative control group (2 wt% erythrocyte suspension in normal physiological saline).

Table 2. Hemolysis test results for the BSA–Ag$_2$S QDs. (Positive control: 2 wt% erythrocyte suspension in deionized water. Negative control group: 2 wt% erythrocyte suspension in normal physiological saline.)

	Negative	Positive	Ag$_2$SQDs (μg ml^{-1})			
			20	40	80	100
Absorbance value	0.057 ± 0.002	1.312 ± 0.017	0.06 ± 0.016	0.077 ± 0.018	0.63 ± 0.004	0.06 ± 0.005
Hemolysis (%)			0.23	1.52	0.46	0.23

due to the extremely low solubility of the Ag$_2$S and the adsorbed proteins on the Ag$_2$S surface. Nanomaterials can form 'coronas' with proteins, which are able to reduce the cytotoxicity of nanomaterials significantly [57]. A naked particle surface might have a much greater nonspecific affinity to the cell surface than a particle hiding behind a protein corona [58]. Therefore, our research provides an alternative and convenient method to design nanomaterials for safe biomedical and environmental applications.

Acknowledgments

References

[1] Lim Y T, Kim S, Nakayama A, Stott N E, Bawendi M G and Frangioni J V 2003 *Mol. Imag.* **2** 50
[2] Welsher K, Liu Z, Sherlock S P, Robinson J T, Chen Z, Daranciang D and Dai H 2009 *Nature Nanotechnol.* **4** 773
[3] Zhang Y, Hong G, Zhang Y, Chen G, Li F, Dai H and Wang Q 2012 *ACS Nano* **6** 3695
[4] Welsher K, Sherlock S P and Dai H 2011 *Proc. Natl Acad. Sci. USA* **108** 8943
[5] O'Connell M J *et al* 2002 *Science* **297** 593
[6] Smith A M, Mancini M C and Nie S 2009 *Nature Nanotechnol.* **4** 710
[7] Crochet J, Clemens M and Hertel T 2007 *J. Am. Chem. Soc.* **129** 8058
[8] Alivisatos A P 1996 *Science* **271** 933
[9] Wu Q and Chu M 2012 *Int. J. Nanomedicine* **7** 3433
[10] Fan J and Chu P K 2010 *Small* **6** 2080
[11] Kim S *et al* 2003 *Nature Biotechnol.* **22** 93
[12] Bakueva L, Gorelikov I, Musikhin S, Zhao X S, Sargent E H and Kumacheva E 2004 *Adv. Mater.* **16** 926
[13] Wehrenberg B L, Wang C and Guyot-Sionnest P 2002 *J. Phys. Chem.* B **106** 10634
[14] Murphy J E, Beard M C, Norman A G, Ahrenkiel S P, Johnson J C, Yu P, Mićić O I, Ellingson R J and Nozik A J 2006 *J. Am. Chem. Soc.* **128** 3241
[15] Xie R, Battaglia D and Peng X 2007 *J. Am. Chem. Soc.* **129** 15432
[16] Harrison M T, Kershaw S V, Burt M G, Eychmüller A, Weller H and Rogach A L 2000 *Mater. Sci. Eng.* B **69/70** 355
[17] Zimmer J P, Kim S W, Ohnishi S, Tanaka E, Frangioni J V and Bawendi M G 2006 *J. Am. Chem. Soc.* **128** 2526
[18] Selvan S T, Tan T T and Ying J Y 2005 *Adv. Mater.* **17** 1620
[19] Wu H, Zhu H, Zhuang J, Yang S, Liu C and Cao Y C 2008 *Angew. Chem. Int. Edn* **47** 3730
[20] Deng Z, Schulz O, Lin S, Ding B, Liu X, Wei X, Ros R, Yan H and Liu Y 2010 *J. Am. Chem. Soc.* **132** 5592
[21] Ding H *et al* 2011 *Nanoscale* **3** 1813
[22] Gao X, Cui Y, Levenson R M, Chung L W K and Nie S 2004 *Nature Biotechnol.* **22** 969
[23] Akamatsu K, Takei S, Mizuhata M, Kajinami A, Deki S, Takeoka S, Fujii M, Hayashi S and Yamamoto K 2000 *Thin Solid Films* **359** 55
[24] Junod P, Hediger H, Kilchör B and Wullschleger J 1977 *Phil. Mag.* **36** 941
[25] Yarema M *et al* 2011 *ACS Nano* **5** 3758
[26] Nowack B 2010 *Science* **330** 1054
[27] Yang X H, Wu Q S, Ding Y P and Zhang G X 2006 *Rare Met. Mater. Eng.* **35** 959
[28] Gao F, Lu Q and Zhao D 2003 *Nano Lett.* **3** 85

[29] Hocaoglu I, Cizmeciyan M N, Erdem R, Ozen C, Kurt A, Sennaroglu A and Acar H Y 2012 *J. Mater. Chem.* **22** 14674

[30] Wang C, Wang Y, Xu L, Zhang D, Liu M, Li X, Sun H, Lin Q and Yang B 2012 *Small* **8** 3137

[31] Gu Y-P, Cui R, Zhang Z-L, Xie Z-X and Pang D-W 2011 *J. Am. Chem. Soc.* **134** 79

[32] Du Y, Xu B, Fu T, Cai M, Li F, Zhang Y and Wang Q 2010 *J. Am. Chem. Soc.* **132** 1470

[33] Goswami N, Giri A, Kar S, Bootharaju M S, John R, Xavier P L, Pradeep T and Pal S K 2012 *Small* **8** 3175

[34] Xie J, Zheng Y and Ying J Y 2009 *J. Am. Chem. Soc.* **131** 888

[35] Tan S J, Campolongo M J, Luo D and Cheng W 2011 *Nature Nanotechnol.* **6** 268

[36] Liu C L *et al* 2011 *Angew. Chem. Int. Edn* **50** 7056

[37] Dameron C T, Reese R N, Mehra R K, Kortan A R, Carroll P J, Steigerwald M L, Brus L E and Winge D R 1989 *Nature* **338** 596

[38] Aizenberg J, Addadi L, Weiner S and Lambert G 1996 *Adv. Mater.* **8** 222

[39] Cha J N, Shimizu K, Zhou Y, Christiansen S C, Chmelka B F, Stucky G D and Morse D E 1999 *Proc. Natl Acad. Sci. USA* **96** 361

[40] Klaus T, Joerger R, Olsson E and Granqvist C G 1999 *Proc. Natl Acad. Sci. USA* **96** 13611

[41] Kröger N, Deutzmann R and Sumper M 1999 *Science* **286** 1129

[42] Douglas T, Strable E, Willits D, Aitouchen A, Libera M and Young M 2002 *Adv. Mater.* **14** 415

[43] Lee S-W, Mao C, Flynn C E and Belcher A M 2002 *Science* **296** 892

[44] Brott L L, Naik R R, Pikas D J, Kirkpatrick S M, Tomlin D W, Whitlock P W, Clarson S J and Stone M O 2001 *Nature* **413** 291

[45] Ma N, Sargent E H and Kelley S O 2008 *J. Mater. Chem.* **18** 954

[46] Peelle B R, Krauland E M, Wittrup K D and Belcher A M 2005 *Langmuir* **21** 6929

[47] Robinson R D, Sadtler B, Demchenko D O, Erdonmez C K, Wang L W and Alivisatos A P 2007 *Science* **317** 355

[48] Anthony S P 2009 *Mater. Lett.* **63** 773

[49] Wen X, Wang S, Xie Y, Li X Y and Yang S 2005 *J. Phys. Chem.* B **109** 10100

[50] Xiang J, Cao H, Wu Q, Zhang S, Zhang X and Watt A A R 2008 *J. Phys. Chem.* C **112** 3580

[51] Li D P, Zheng Z, Lei Y, Yang F L, Ge S X, Zhang Y D, Huang B J, Gao Y-H, Wong K W and Lau W-M 2011 *Chem. Eur. J.* **17** 7694

[52] Zhang B, Ye X, Dai W, Hou W and Xie Y 2006 *Chem. Eur. J.* **12** 2337

[53] Kartio I, Laajalehto K, Suoninen E, Karthe S and Szargan R 1992 *Surf. Interface Anal.* **18** 807

[54] Kong J and Yu S 2007 *Acta Biochim. Biophys. Sin.* **39** 549

[55] Cheng F Y, Su C H, Yang Y S, Yeh C S, Tsai C Y, Wu C L, Wu M T and Shieh D B 2005 *Biomaterials* **26** 729

[56] Kainthan R K, Gnanamani M, Ganguli M, Ghosh T, Brooks D E, Maiti S and Kizhakkedathu J N 2006 *Biomaterials* **27** 5377

[57] Cedervall T, Lynch I, Lindman S, Berggård T, Thulin E, Nilsson H, Dawson K A and Linse S 2007 *Proc. Natl Acad. Sci. USA* **104** 2050

[58] Verma A, Uzun O, Hu Y, Hu Y, Han H-S, Watson N, Chen S, Irvine D J and Stellacci F 2008 *Nature Mater.* **7** 588